Universality of the electronic structure from a half-filled CuO$_2$ plane

F. Ronning,* C. Kim,† K. M. Shen, N. P. Armitage,§ A. Damascelli,‡ D. H. Lu, D. L. Feng,‡ and Z.-X. Shen
Department of Physics, Applied Physics and Stanford Synchrotron Radiation Laboratory, Stanford University, Stanford, California 94305

L. L. Miller
Department of Physics, Iowa State University, Ames, Iowa 50011

Y.-J. Kim and F. Chou
Department of Physics, Massachusetts Institute of Technology, Cambridge, Massachusetts 02139

I. Terasaki
Department of Applied Physics, Waseda University, Tokyo 169-8555, Japan

We present angle-resolved photoemission spectroscopy data from insulating $A_2CuO_2X_2$ ($A =$ Sr, Ca; $X =$ Cl, Br), $Sr_2Cu_3O_4Cl_2$, and $Bi_2Sr_2MCu_2O_8$ ($M =$ Er, Dy) single crystals, which illustrate that the low-energy electronic structure of the half-filled cuprates are independent of the apical atom. By performing a photon energy dependent study on $Ca_2CuO_2Cl_2$, we are able to distinguish between features which are intrinsic and those which are a result of the photoemission matrix elements. We find that the dispersion is independent of photon energy, while an asymmetry in the electron occupation probability across the antiferromagnetic zone boundary is robust to variations in photon energy. Finally, we show that the d-wave-like dispersion which exists in the insulator along the antiferromagnetic zone boundary does not precisely fit the simple d-wave functional form near the nodal direction.

I. INTRODUCTION

One approach in unraveling the mysteries of the high-T_c superconductors is to understand how the electronic structure evolves from an antiferromagnetic insulator to a superconductor upon doping. The first step is then to understand the insulator to metal transition. Although Mott qualitatively described how a material, predicted by band theory to be a metal, would in fact be an insulator,[1] it remains unclear as to how the details of the electronic structure evolve from a half-filled metal to a Mott insulator. Questions such as how does the gap open, and what happens to the information contained in the occupation probability $n(\mathbf{k})$ when strong correlations drive the system insulating need to be answered. The technique of angle-resolved photoemission spectroscopy (ARPES) is a natural choice to do this.

Of course, with every well posed question, there are experimental challenges which make it difficult to answer these questions. $La_{2-x}Sr_xCuO_4$ is one system which has been successfully grown from half filling to heavily overdoped; however, ARPES results on these crystals remain somewhat uncertain as illustrated by the extremely broad spectra of La_2CuO_4. (Ref. 2) $Nd_{2-x}Ce_xCuO_4$ is another system which spans a similar doping range, and has attempted to answer the above questions;[3,4] however, it is not clear whether the results can be generalized to include the hole-doped cuprates. $YBa_2Cu_3O_{6+\delta}$, which can cover the range of half filling to optimal doping, might appear as the next suitable candidate, but the presence of a surface state and the existence of one-dimensional chains have clouded the interpretation of its bulk electronic structure.[5] The $Bi_2Sr_2CaCu_2O_{8+\delta}$ (Bi2212) system, with its extremely good cleavage plane, has been

ideal for ARPES. For precisely this reason, the majority of ARPES data on the high T_c's to date have come from Bi2212. Unfortunately, high-quality Bi2212 crystals at very low dopings have not been achieved. On the other hand, $A_2CuO_2Cl_2$ ($A =$ Sr,Ca) also cleaves extremely well and gives high-quality ARPES data comparable to that seen in optimally doped Bi2212, but in this case, single crystals have only been available at half filling. As a result, there exists no perfect system to study the electronic structure from the antiferromagnetic insulator to the heavily over doped metal in the hole-doped cuprates.

The solution has been to make the reasonable assumption that the low-energy physics of the Bi2212 and $A_2CuO_2Cl_2$ (ACOC) systems are identical due to the fact that the CuO$_2$ planes are common to both structures. Thus the entire doping range can be studied. However, these two systems also have several differences. $Sr_2CuO_2Cl_2$ (SCOC) and $Ca_2CuO_2Cl_2$ (CCOC) have a Cu-O-Cu distance of 3.97 Å and 3.87 Å, respectively,[6] compared to 3.83 Å for Bi2212,[7] and they also do not possess the orthorhombic distortion and superstructure effects which plague Bi2212. Finally, the most striking difference in ACOC is that the apical oxygen has been replaced with a chlorine atom. It is important to test whether or not these differences can have an effect on the low-energy electronic structure.

In this paper, we will validate the assumption that low-energy ARPES data on the oxyhalides are indeed representative of photoemission from a generic, half-filled CuO$_2$ plane, and thus may be reasonably compared with ARPES data on hole-doped Bi2212. This will be done by showing that replacing the apical chlorine with the larger and less electronegative bromine has no effect on the low-energy

electronic structure. Furthermore, it will also be shown that heavily underdoped Bi2212 near half filling, despite having relatively poor spectral quality, is qualitatively consistent with the results on the oxyhalides. Finally, ARPES on $Sr_2Cu_3O_4Cl_2$, which contains an additional copper atom in every other CuO_2 plaquette, demonstrates that the lowest-lying excitations attributed to a Zhang-Rice singlet[8] are surprisingly unaffected by even a seemingly large modification of the CuO_2 plane.

Having shown that the ARPES results of the half-filled Mott-insulating cuprate are not system dependent, we will turn our attention in the latter half to extracting the physics of the half-filled CuO_2 plane contained in the single-particle spectral function, $A(\mathbf{k}, \omega)$. Because matrix elements modulate the measured photoemission intensity, it is important to distinguish which features of the data are intrinsic and which are extrinsic. However, photon energy (E_γ) dependent studies designed specifically to test the influence of the matrix element on both the dispersion $E(\mathbf{k})$,[9,10] and the intensity $n(\mathbf{k})$,[11] have had conflicting reports on the magnitude of variations caused by matrix elements. So to test whether or not the dispersion and the $\mathbf{k}$ dependence of the spectral weight are impressive manifestations of matrix element modulations, we have performed ARPES $n(\mathbf{k})$ mappings over the entire Brillouin zone for five different photon energies, and examined the $(0,0)$ to (π, π) cut for 13 photon energies. We find that the dispersion is independent of the photon energy as one might expect, and that with few exceptions, the remnant Fermi surface[12] is robust despite observing strong variations in spectral weight caused by matrix elements.

With an understanding of the matrix element we can finally turn our attention to the physics. Specifically, we will focus on the d-wave-like dispersion found in the insulator.[12] This observation allows for a natural connection between the d-wave form of the high-energy pseudogap seen in underdoped Bi2212 and the dispersion of the insulator as first suggested by Laughlin.[13] This connection is particularly intriguing in light of the fact that the high-energy pseudogap and the low-energy pseudogap appear to be correlated.[14] The latter of which is directly related to the superconducting gap, thus linking antiferromagnetism which is responsible for the dispersion of the insulator to d-wave superconductivity.

The original ARPES dispersion data on CCOC left some ambiguity as to whether or not the detailed dispersion near the node exactly fit the d-wave functional form. A linear dispersion at the node of the form $E(\pi/2, \pi/2) - E(\mathbf{k}) \propto \|\mathbf{k} - (\pi/2, \pi/2)\|$ is highly nontrivial and several theories which attempt to connect the insulator to the superconductor predict precisely such a discontinuity in the derivative of the dispersion at the node.[13,15,16] However, the t-J model with next nearest-neighbor hopping terms t' and t'', which correctly describes gross features of the dispersion, has a functional form of $\cos 2k_x a + \cos 2k_y a$ which is analytic at $k_x = k_y$. To investigate this issue, we performed ultrahigh resolution ARPES experiments along the antiferromagnetic Brillouin zone to determine the exact nature of the dispersion near $k_x = k_y$. From this data we find that the dispersion near the node is nonlinear and thus cannot be fit by the simple d-wave

functional form of $|\cos k_x a - \cos k_y a|$.

The paper is organized as follows. Section II presents the experimental details. Sections III–VI present photoemission results from the various insulating parent cuprates illustrating that the low-energy spectra are independent of the apical site. Section VII is a photon energy dependent investigation of CCOC. Section VIII compares the dispersion of CCOC with the pure d-wave functional form. Section IX discusses the experimental results with regard to current theoretical understanding after which we conclude.

II. EXPERIMENT

$A_2CuO_2X_2$ (A = Sr, Ca; X = Cl, Br), $Sr_2Cu_3O_4Cl_2$, and $Bi_2Sr_2MCu_2O_8$ (M = Er, Dy) single crystals were grown by a slow cool flux method.[17,18] ARPES experiments were performed at beamlines V-3 and V-4 of the Stanford Synchrotron Radiation Laboratory. The beamline V-4 system is capable of achieving an energy and angular resolution better than 15 meV and 0.25°. However, for the majority of this work such a high resolution is not necessary due to the extremely broad features which are being studied. Thus, the high resolution is only occasionally utilized, while the remaining data presented use a resolution of $\leq$70 meV and $\pm$1°. Crystals were oriented prior to the experiment by Laue back reflection, and cleaved *in situ* at a base pressure better than 5×10^{-11} torr. The photon flux was varied to determine whether or not the insulating sample was charging. If it was, then the sample temperature was raised when possible to eliminate this effect. A line shape which is independent of the photon flux is taken as a proof that there is no charging despite the fact that the samples are insulators. Slight charging is observed for the $Ca_2CuO_2Br_2$ and $Sr_2Cu_3O_4Cl_2$ samples at room temperature, but the results were reproducible and the spectra simply shifted to higher binding energy with increased flux indicating a uniform potential barrier formed due to charging.

We also note that the minimum binding energy of an insulator can vary up to 1 eV from cleave to cleave even in the absence of any charging. The reason for this is not known with certainty, but is likely due to different pinning sites for different cleaves. For the oxychlorides, we typically find the centroid of the minimum binding-energy feature to lie between 0.5 and 0.8 eV below the chemical potential which is determined by the E_F of a reference gold sample in electrical contact.

III. $Sr_2CuO_2Cl_2$ AND $Ca_2CuO_2Cl_2$

Figure 1 presents a comparison between SCOC and CCOC along the high-symmetry directions. The two are nearly identical. This is to be expected as Sr and Ca are isovalent and lie between the CuO_2 planes. From $(0,0)$ to (π, π) they show a feature which emerges from the background, disperses towards the chemical potential, reaches a maximum at $(\pi/2, \pi/2)$ and then loses weight rapidly as it pushes back to higher binding energy.[19] We note that the centroid of the lowest-energy excitation at $(\pi/2, \pi/2)$ still lies well below the chemical potential (off scale), indicative
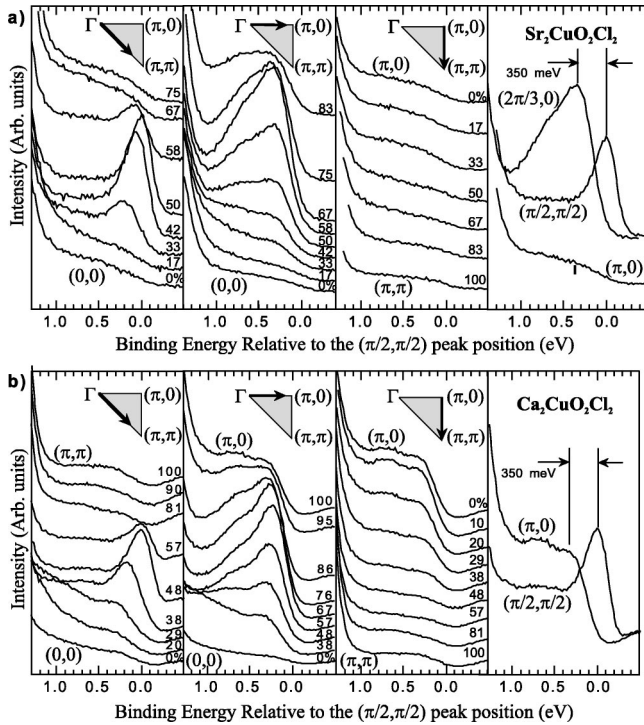
FIG. 1. EDC's of $Sr_2CuO_2Cl_2$ (a) and $Ca_2CuO_2Cl_2$ (b) along the high-symmetry direction indicated in the insets. The final panel indicates the magnitude of the d-wave-like dispersion seen in the oxyhalides, and the difference in line shape exhibited as a function of **k**. The measurement conditions were $T=150$ K, $E_\gamma=22.4$ eV and $T=100$ K, $E_\gamma=25.2$ eV for $Sr_2CuO_2Cl_2$ and $Ca_2CuO_2Cl_2$, respectively.

of the fact that these crystals are Mott insulators. Along the (0,0) to $(\pi,0)$ cut a more intense and significantly more asymmetric peak is observed. Under certain experimental conditions it becomes clear that this strong asymmetry is due to the presence of a second feature which lies ≈ 600 meV below the main band.[20] The dispersion of this second feature appears similar to that of the lower binding-energy feature, although the intensity is not. The feature along the $(\pi,0)$ cut does not show much dispersion, and lies ≈ 350 meV below the maximum in dispersion at $(\pi/2,\pi/2)$. In spectra where the peak positions are not as clear, we will attempt to make a quantitative comparison by taking the minimum of the second derivative of the spectra. We do not present any detailed fits of the spectra due to a lack of theoretical understanding of the broad spectral line shapes inherent to the half-filled cuprates. We note that the broad spectral line shapes of the half-filled cuprates are intrinsic properties of the spectra, and not a result of the sample charging. As stated above, this is confirmed in ACOC by varying the photon flux and observing no change in the spectra.

The one significant difference between SCOC and CCOC is the observed spectral weight at $(\pi,0)$ in CCOC which is suppressed in SCOC. On going from $(\pi,0)$ to (π,π) it can be seen that this weight vanishes quickly. Although it is not clear why the matrix elements would favor CCOC over SCOC in the $(\pi,0)$ region, it is this difference which facili-
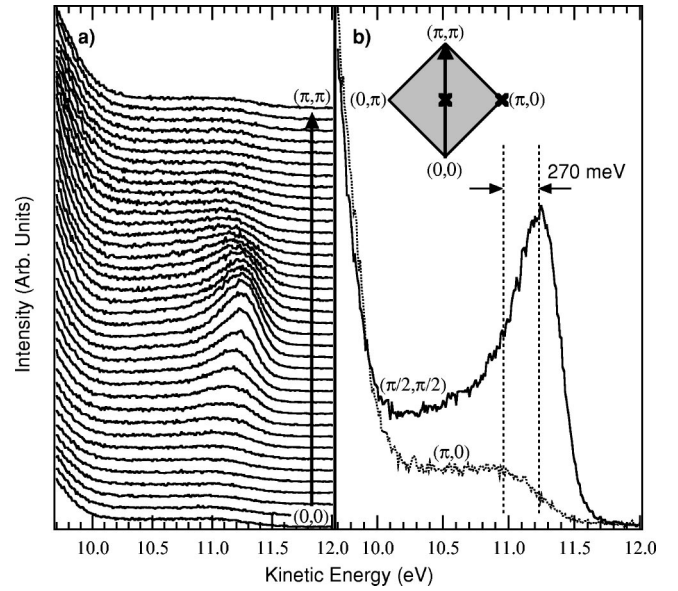

FIG. 2. (a) EDC's of $Ca_2CuO_2Br_2$ from (0,0) to (π,π) taken with 16.5-eV photons at $T=372$ K. (b) Comparison of $(\pi/2,\pi/2)$ (solid line) and $(\pi,0)$ (dotted line). The dashed lines mark the positions of maximum curvature.

tated the identification of a remnant Fermi surface in CCOC, which was not observed in previous studies on SCOC.[12]

One of the most significant features of the insulator is the dispersion between $(\pi/2,\pi/2)$ and $(\pi,0)$. There are two aspects to notice in the right most panels of Fig. 1. The most important is clearly the difference of roughly 350 meV in dispersion. This is the magnitude of the d-wave-like modulation seen in the insulator. The second is the strong difference in line shape. At $(\pi/2,\pi/2)$ the spectra show a clear peak that resembles a quasiparticlelike peak, albeit with a *very* large width (~ 300 meV), while at $(\pi,0)$, the spectra merge more continuously into the high-energy background, somewhat resembling a step function. These will be the benchmarks to which the other compounds will be compared in determining whether or not the data from SCOC and CCOC are representative of a single half-filled CuO_2 plane.

IV. $Ca_2CuO_2Br_2$

The biggest difference between ACOC and other high-T_c cuprates is the presence of chlorine as opposed to oxygen in the apical site. To see whether or not the apical site has an effect on the electronic structure, we present in Fig. 2 the ARPES data from $Ca_2CuO_2Br_2$ where bromine has replaced chlorine in the apical site. From band theory calculations the binding energy of the apical orbital is -3.4 eV, -2.8 eV, and -2.6 eV for $Ca_2CuO_2Cl_2$, $Ca_2CuO_2Br_2$ (CCOB), and La_2CuO_4, respectively,[21] which suggests that CCOB is a suitable candidate to determine the effect of the apical chlorine as compared with an apical oxygen on the low-energy electronic structure. On the cut from (0,0) to (π,π) a dispersive feature is clearly observed with a minimum in binding energy at $(\pi/2,\pi/2)$ and an overall bandwidth of ≈ 300 meV. In panel (b) the spectra at $(\pi/2,\pi/2)$ and $(\pi,0)$
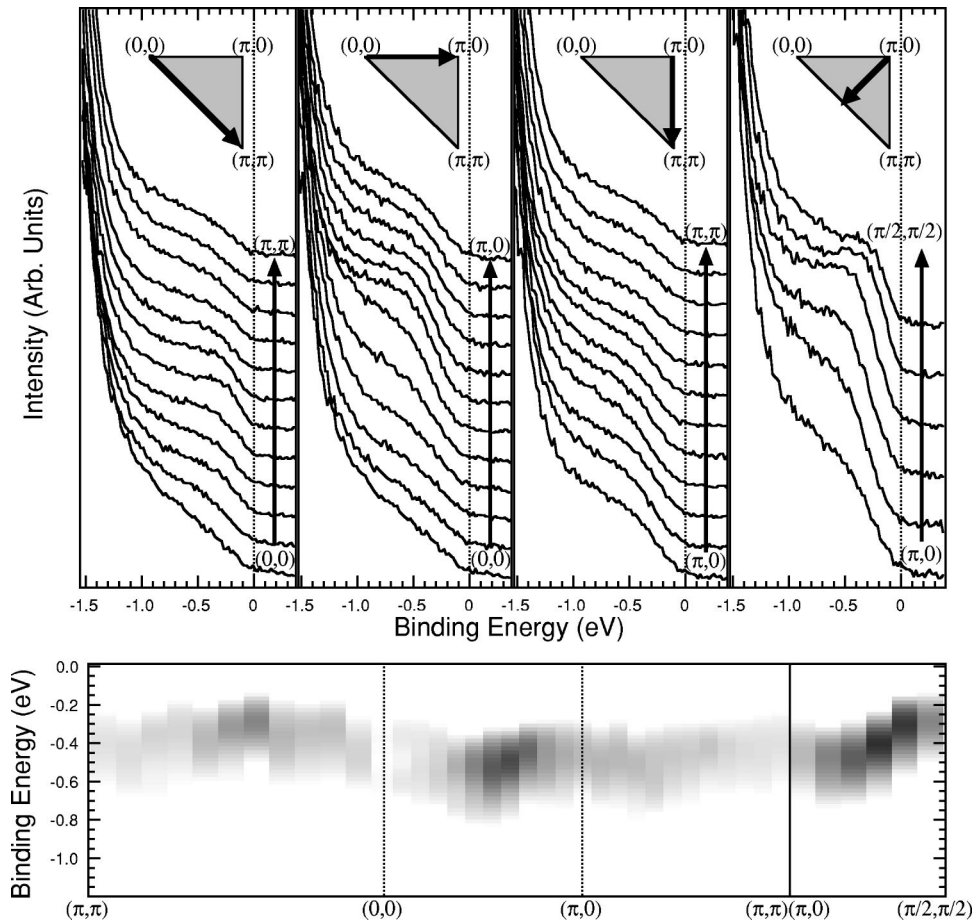
FIG. 3. EDC's of $Bi_2Sr_2ErCu_2O_8$ along the high-symmetry directions as indicated in the cartoons. Below is a plot of the second derivative of the above EDC's, from which one can trace out the dispersion. $E_\gamma = 22.4$ eV and $T = 100$ K.

are compared. These data look almost identical to those from CCOC, which are shown in Fig. 1. Specifically, the line shape at $(\pi/2,\pi/2)$ is quite sharp and well defined as compared to the broad feature seen at $(\pi,0)$. The energy difference of 270 meV (determined by the minimum of the second derivative of the corresponding spectra) is also consistent with that seen in CCOC. We also took a limited amount of data on $Sr_2CuO_2Br_2$ (not shown). The general features of $Sr_2CuO_2Br_2$ were consistent with that of the other oxyhalides, although significant charging was observed. The data on the oxybromides suggest that the low-energy excitations are relatively independent of the apical atoms and the observed spectral function in ACOC thus originates from the half-filled CuO_2 plane. Consequently, the comparison of ARPES data on ACOC at half filling with Bi2212 data at finite doping seems valid.

V. $Bi_2Sr_2ErCu_2O_8$ AND $Bi_2Sr_2DyCu_2O_8$

Of course, as mentioned previously, the ideal scenario to examine the doping evolution is to study the same system through the entire doping range. Therefore, we also present Er and Dy-doped Bi2212 crystals grown near half filling. Figures 3 and 4 show the energy distribution curves (EDC's) for these samples along the high-symmetry directions. The low-energy features are not nearly as well defined as in the oxyhalides; however, a clear shoulder does emerge from the background. The poor definition of these features is consis-

tent with previous studies on underdoped Bi2212, which show that the low-energy excitation spectra become smeared out as one proceeds toward half filling in this system.[22,23] This is precisely the reason why ARPES data on the oxychlorides have been so valuable in understanding the problem of a single hole in an antiferromagnet. The reason for the relatively poor spectral quality of heavily underdoped Bi2212 is an open question, although it is possibly simply an issue of sample quality, such as lattice strain.

Examining the low-energy spectra from $(0,0)$ to (π,π) of Er-doped Bi2212 we see that the shoulder is most pronounced at $(\pi/2,\pi/2)$ with a minimum binding energy of -0.27 eV. From $(0,0)$ to $(\pi,0)$ the shoulder develops at higher binding energy with a value of -0.49 eV at $(\pi,0)$ and then disappears again as one travels from $(\pi,0)$ to (π,π). Although there is significant ambiguity in identifying the binding energy of these features, the fact that the shoulder has a dispersion of roughly 0.22 eV between $(\pi,0)$ and $(\pi/2,\pi/2)$ can be clearly seen in the final panel. The second derivative of the spectra from which the above values are attained are also presented in Fig. 3. One can see that the dispersion found with this method reproduces the above description. Results on Dy-doped Bi2212 shown in Fig. 4 clearly mimic the behavior seen in the Er-doped Bi2212 including the 0.22-eV difference in energy between $(\pi/2,\pi/2)$ and $(\pi,0)$. The overall features of the dispersion and the resulting energy difference of roughly 220 meV between $(\pi/2,\pi/2)$ and $(\pi,0)$ in Er- and Dy-doped Bi2212 are quali-
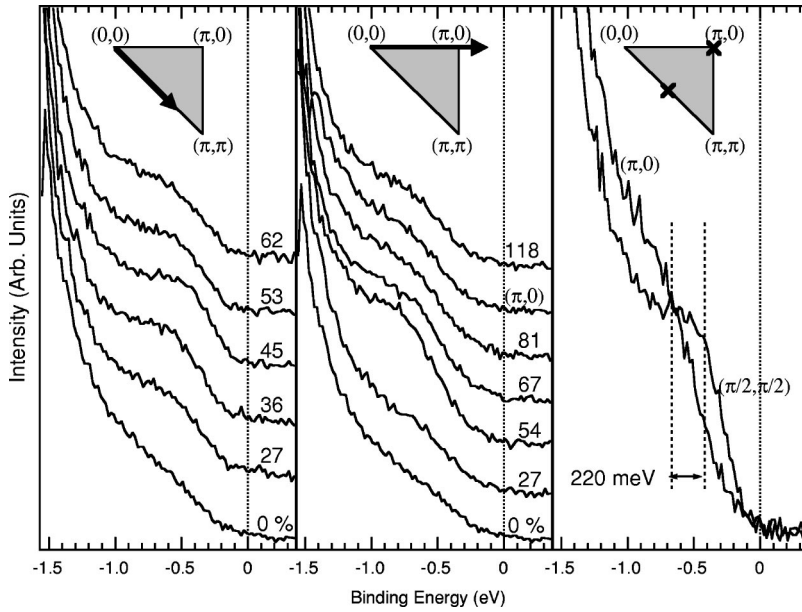
FIG. 4. EDC's of $Bi_2Sr_2DyCu_2O_8$ along the high-symmetry directions as indicated in the cartoons. $E_\gamma = 22.4$ eV and $T = 75$ K. The dashed lines in the right panel mark the positions of maximum curvature.

tatively consistent with the dispersion and the 350-meV d-wave-like modulation seen in CCOC. We suspect that the quantitative difference between Bi2212 and ACOC may be simply due to the poor definition of spectral features of the former, but we cannot rule out the possibility that it is an intrinsic difference between the two samples. Nevertheless, even with the poor spectral definition in heavily underdoped Bi2212, the electronic structure is still qualitatively consistent between the oxyhalide and Bi2212 systems. This result along with our data on CCOB, justifies the long-standing assumption that the ARPES data from SCOC and CCOC are representative of a half-filled CuO_2 square lattice.

VI. $Sr_2Cu_3O_4Cl_2$: Cu_3O_4 PLANE

$Sr_2Cu_3O_4Cl_2$ is a particularly remarkable example of the apparent robustness of the structure of the lowest-energy excitations. This system deviates from the other cuprates due to an additional Cu atom located in every other CuO_2 plaquette resulting in an in-plane stoichiometry of Cu_3O_4. The resulting crystal structure has a unit cell twice as large as in $Sr_2CuO_2Cl_2$ and rotated by 45° (see Fig. 5). Thus $(\pi,0)$ of the CuO_2 unit cell is now equivalent to (π,π) in the Cu_3O_4 system, and similarly $(\pi/2,\pi/2)$ for $Sr_2CuO_2Cl_2$ is equivalent to $(\pi,0)$ for $Sr_2Cu_3O_4Cl_2$. However, instead of presenting results in the new Cu_3O_4 basis, we will continue to present all momentum values in the original CuO_2 basis. This will make for a simpler comparison between the two systems.

A sample valence-band spectra of $Sr_2Cu_3O_4Cl_2$ at $(\pi/2,\pi/2)$ are shown in Fig. 6. In fact it is very similar to the valence band of $Sr_2CuO_2Cl_2$ at $(\pi/2,\pi/2)$.[10] We will, however, continue to focus on the "foot" of the valence band, which contains the low-energy excitations. The following panel examines the low-energy excitation spectra at two equivalent points: $(+\pi/2,+\pi/2)$ and $(+\pi/2,-\pi/2)$. Since

the polarization of the incident light is horizontal, the suppression of spectral weight at $(+\pi/2,-\pi/2)$ relative to $(+\pi/2,+\pi/2)$ indicates that the wave function at $(\pi/2,\pi/2)$ is odd with respect to a mirror plane at 45° to the Cu-O bond direction. This observation is consistent with the state having a $d_{x^2-y^2}$ orbital character.

In Fig. 7, two perpendicular cuts through $(\pi/2,\pi/2)$ are shown. Note that the lowest-energy feature is most well defined near $(\pi/2,\pi/2)$, the dispersion is isotropic about its maximum at $(\pi/2,\pi/2)$, and as can be seen in the final panel, $(\pi,0)$ lies ≈ 320 meV below $(\pi/2,\pi/2)$, although significant uncertainty exists in the peak position. These results, including the polarization dependence, are identical to the case of ACOC.[10] They are also consistent with earlier reports on the isostructural compound $Ba_2Cu_3O_4Cl_2$ taken at a higher photon energy.[24,25] We confirm the observation that the spectral features about $(\pi/2,\pi/2)$ have a remarkable resemblance to those in $Sr_2CuO_2Cl_2$. It is astounding that the properties of the Zhang-Rice singlet seen in ACOC are almost undisturbed
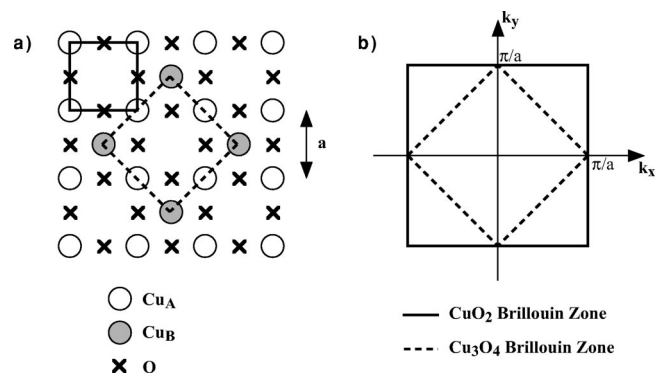

FIG. 5. Real space (a) and reciprocal space (b) cartoons of the unit cell of Cu_3O_4 (dashed line). The unit cell of the CuO_2 (solid line) is shown for comparison.
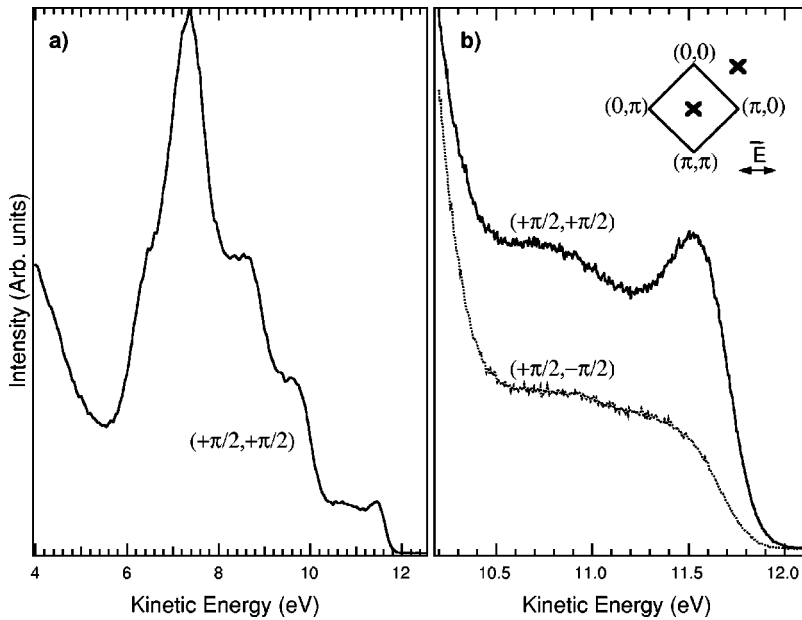
FIG. 6. (a) Valence-band spectra of $Sr_2Cu_3O_4Cl_2$ at $(+\pi/2,+\pi/2)$. b) An expanded view of the low-energy spectra. A comparison of the spectra at $(+\pi/2,+\pi/2)$ (solid line) and $(+\pi/2,-\pi/2)$ (dotted line) indicates that the wave function responsible for the low-energy excitations is odd with respect to a 45° line relative to the Cu-O bond direction. $E_\gamma = 16.55$ eV and $T = 293$ K.

by the drastic change to the CuO_2 lattice in the case of $Sr_2Cu_3O_4Cl_2$.

VII. E_γ DEPENDENCE ON $E(k)$ AND $n(k)$

Having shown that the low-energy spectra of a half-filled CuO_2 plane are independent of the material system being studied, we next attempt to separate the features of the data which are representative of the single-particle spectral function, $A(\mathbf{k},\omega)$, from those which are a result of the matrix elements. Unfortunately, extracting the single-particle spectral function from ARPES measurements is difficult due to the fact that the measured photoemission intensity under the sudden approximation is a product of the occupied single particle spectral function and the matrix element. In interacting electron systems, it is impossible to calculate the matrix elements exactly, thus further complicating the ARPES

analysis. Although we note that symmetry arguments can be very powerful in understanding some properties of the matrix element,[10] in general it is a function of the experimental geometry, photon energy, and the electronic wave function. Since its details are not well understood, the objective in a given photoemission study must be to focus on only those features of the data which are robust against variations in the experimental conditions.

Here we present a photon energy dependence study to extract the intrinsic $E(\mathbf{k})$ and $n(\mathbf{k})$ structure from the raw ARPES data, which is modulated by the matrix element. On a single cleave we measured EDC's along the nodal direction for 13 different photon energies from 14.5 to 33 eV, which are shown in Fig. 8. The morphologies of the spectra are similar to one another. There are two aspects we wish to address. First, the minimum binding energy occurs near $(\pi/2,\pi/2)$ for all the photon energies studied, and second, with a few exceptions, the intensity profile begins to lose weight before the minimum in binding energy is reached [photon energies of 16.5, 32, and 33 eV are the exceptions where the intensity is symmetric about $(\pi/2,\pi/2)$]. We will address the latter point in more detail below.

To check if the dispersion is indeed independent of photon energy we plot the peak position versus k for each photon energy in Fig. 9(a). The peak positions were found by taking the minimum of the second derivative of each spectra. One can see that to within our experimental limits, which were determined by the reproducibility of the dispersion on subsequent scans under identical conditions and are given by the width of the blue bar, the dispersion is independent of photon energy. This agrees with most of the previous reports on SCOC,[19,20,26] including one very detailed, recent study,[10] but contrasts with the results from Refs. 11, and 27, the former of which report that the minimum binding-energy position shifts by $\approx 10\%$ of the $(0,0)$ to (π,π) distance to $(0.39\pi, 0.39\pi)$ when using 35-eV photons (note that this is outside of our momenta error bars). They attribute this
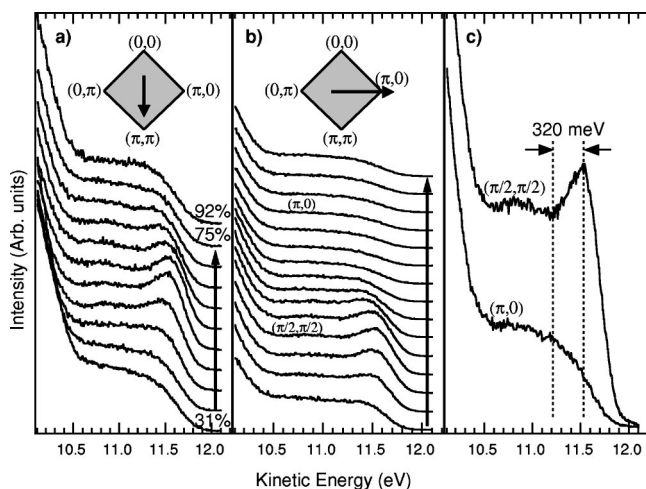

FIG. 7. (a) and (b) EDC's of $Sr_2Cu_3O_4Cl_2$ along two high-symmetry directions as indicated in the inset. (c) Comparison of the spectra at $(\pi/2,\pi/2)$ and $(\pi,0)$. $E_\gamma = 16.5$ eV and $T = 293$ K.
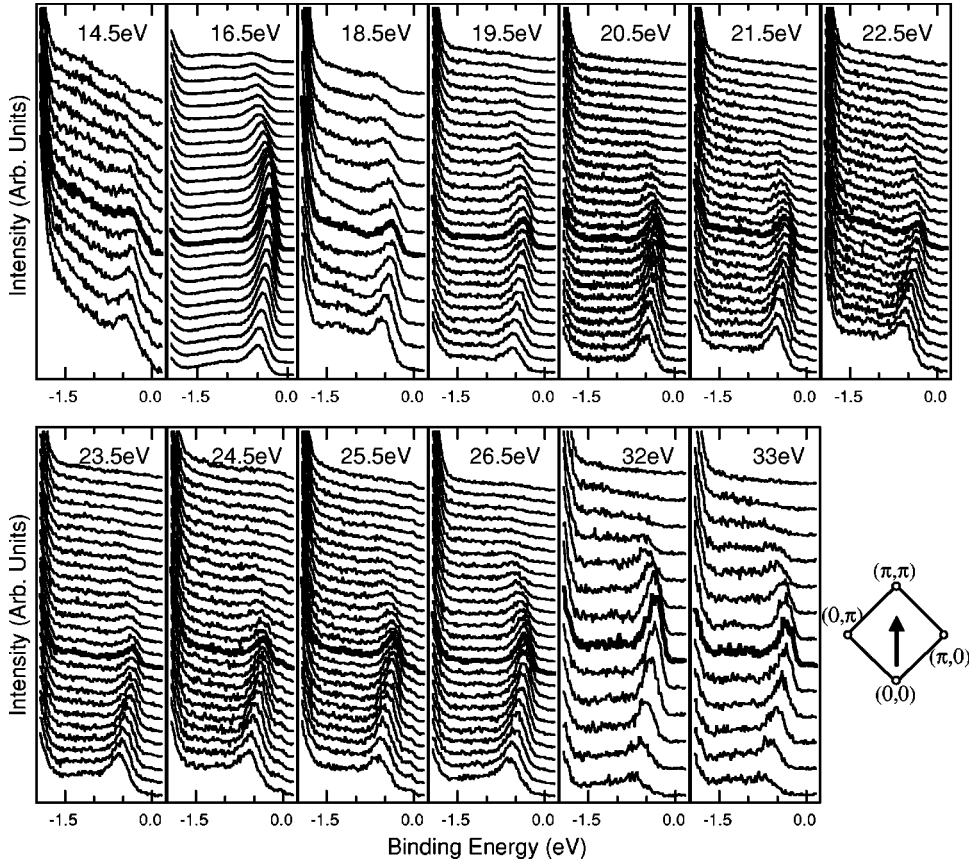
FIG. 8. EDC's from a single cleave of CCOC along $\Gamma \rightarrow (\pi, \pi)$ for 13 different photon energies indicated in each panel, respectively. The bold spectra indicate $(\pi/2, \pi/2)$. The angular separation between the top and bottom spectra in each panel is $11.4°$ with an energy resolution, $\Delta E \leq 50$ meV. $T = 200$ K.
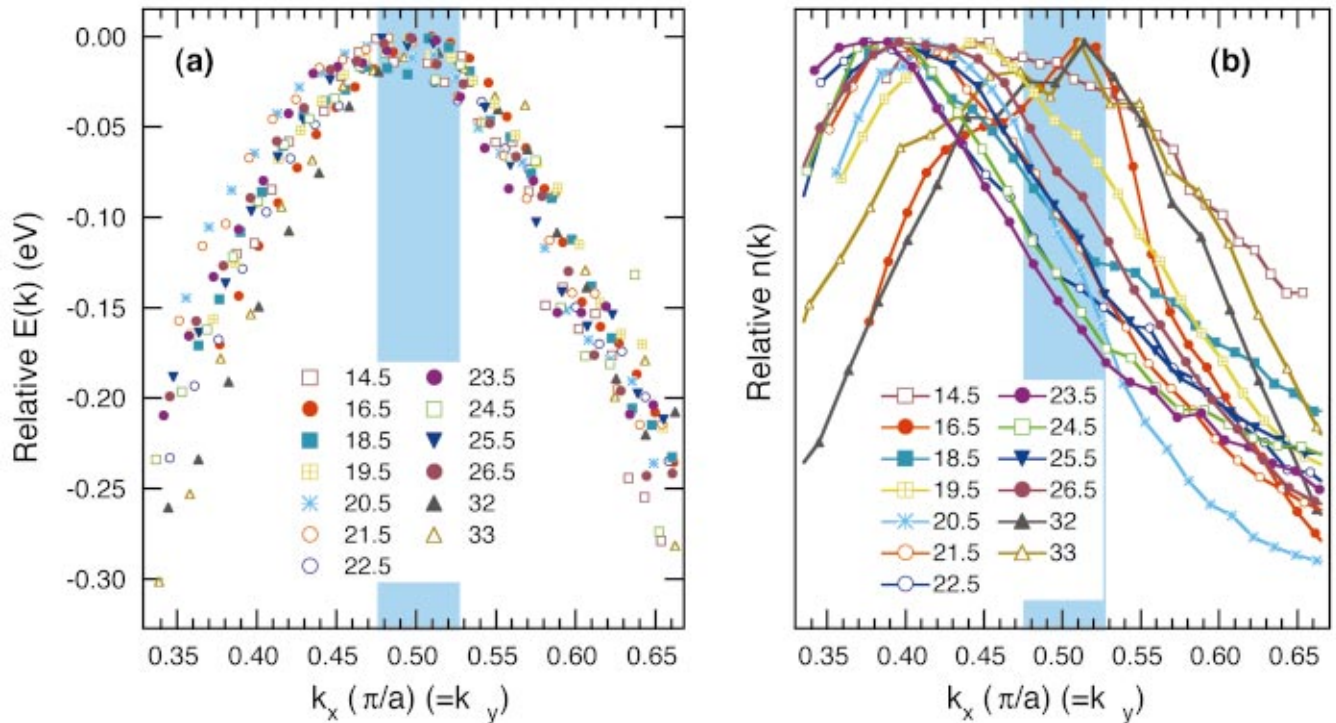

FIG. 9. (Color) (a) $E(\mathbf{k})$ obtained along the nodal direction from the 13 photon energies presented in Fig. 8. $E(\mathbf{k})$ is determined by the minimum of the second derivative of the EDC's. (b) $n(\mathbf{k})$ obtained from the same data by integrating the EDC's over an 800-meV window. The maxima of each curve were normalized to each other for display. The shaded bar represents the momenta error bars.
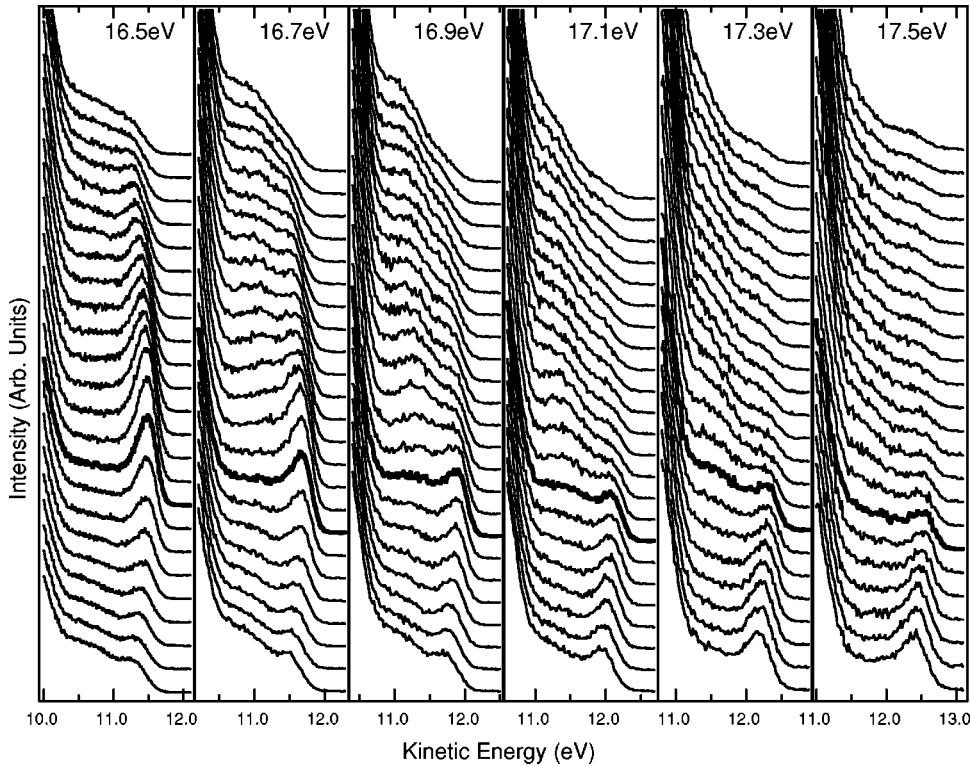
FIG. 10. EDC's from a single cleave of CCOC along the nodal direction for $E_\gamma = 16.5$ eV to $E_\gamma = 17.5$ eV as indicated in each panel. The bold spectra indicate $(\pi/2, \pi/2)$. The angular separation between the top and bottom spectra in each panel is 13° with an energy resolution, $\Delta E = 70$ meV. $T = 293$ K.

change to matrix elements, where the dependence on binding energy varies as a function of photon energy.

Aside from indicating the expected two-dimensional nature of the dispersion, our photon energy dependence has also clearly resolved the presence of a second component in the low-energy electronic structure of the half-filled insulator.[20] Figure 10 presents EDC's in the nodal direction for six photon energies from 16.5 eV to 17.5 eV. Aside from the feature typically associated with the Zhang-Rice singlet, a second component is observed at ≈ 600 meV higher binding energy. In the nodal direction this feature is most clearly resolved at 17 eV. From this data it is clear that when attempting to model the data on the insulator, one cannot simply treat the high-energy spectral weight as a featureless background. Although the dispersion of this feature is difficult to track, it appears to mimic the dispersion of the lowest-energy feature. The strong influence of matrix elements and a lack of understanding of the origin of the spectral line shapes prevent us from extracting detailed information on this high-energy feature and its evolution with photon energy. One possible origin of this feature is from string resonances.[28] String resonances occur when a hole, created in an antiferromagnetic background, experiences a confining potential due to the energy cost associated with disrupting the antiferromagnetic order as it hops away from its original location. The lowest-energy state for the hole in this potential corresponds to the Zhang-Rice singlet, while the first excited state is predicted to lie roughly $1.8(J/t)^{2/3} \approx 0.5$ eV higher in energy.[29] Although we are not certain of the origin of the higher-energy feature, the string resonance concept provides an intriguing possibility for further study.

Having examined the dispersion, we now look at the more difficult problem of extracting the underlying $n(\mathbf{k})$ structure.

It is of particular interest to determine whether or not the underlying intensity profile of $A(\mathbf{k}, \omega)$ has an asymmetry with respect to the antiferromagnetic zone boundary, as this would put constraints on the valid coupling regime for different models.[28,30] For the majority of data shown in Fig. 8 we noticed that the intensity of the lowest-energy excitation begins to lose weight before $(\pi/2, \pi/2)$. By examining the image plot of a representative set of spectra (as done in Fig. 11), this effect can be seen to be quite dramatic. This has also been observed previously by several authors with isolated photon energies.[9,19,20,26,27] In Fig. 9(b) the $n(\mathbf{k})$ curves obtained by integrating the EDC's from -0.5 to 0.3 eV relative to the valence-band maximum for each photon energy are shown. In presenting $n(\mathbf{k})$ we implicitly use the sudden approximation to extract the momentum distribution function $n(\mathbf{k})$ from ARPES data via the relation $n(\mathbf{k}) = \int A(\mathbf{k}, \omega) f(\omega) d\omega$, where $f(\omega)$ is the Fermi function.[31] We note here that the experimental quantity measured is not precisely $n(\mathbf{k})$, as the photoemission intensity is weighted by the matrix element and the integration window is limited due to the presence of additional bands. The energy integration window was chosen so as to minimize the contribution from the second component seen at higher binding energy, but we note that the results are qualitatively independent of the specific energy window chosen.

Clearly, with the exception of 16.5, 32, and 33 eV, the intensity profile peaks well before $(\pi/2, \pi/2)$, and drops rapidly as one crosses the antiferromagnetic zone boundary at $(\pi/2, \pi/2)$. The fact that 16.5-, 32-, and 33-eV data can differ so dramatically is an evidence of what the matrix elements can do. If the underlying spectral function were symmetric about $(\pi/2, \pi/2)$, then one would expect that the distribution
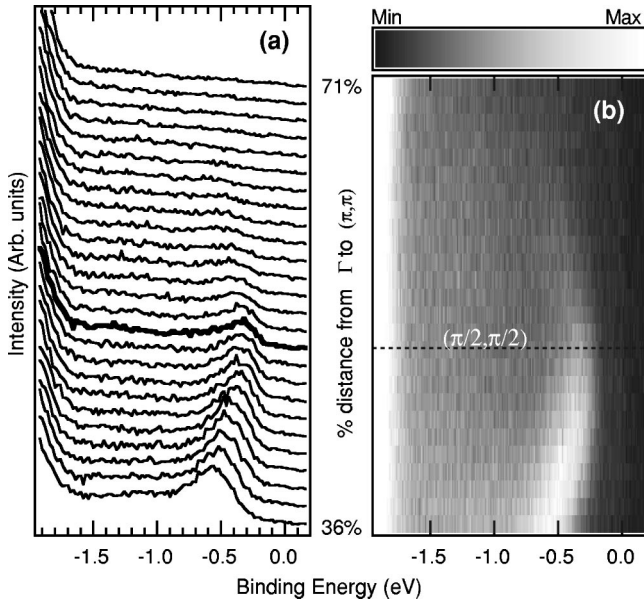
FIG. 11. (a) EDC's and (b) corresponding image plot of CCOC taken along the nodal direction with 23.5 eV photons. The bold spectra indicate $(\pi/2,\pi/2)$, and $T=200$ K.

of curves in Fig. 9(b) would be evenly distributed about $(\pi/2,\pi/2)$. This is the case for a similar study on SCOC, which used five photon energies from 20 to 24 eV.[11] They observe the intensity profile to be more heavily weighted towards (0,0) at $E_\gamma=24$ eV, which then gradually shifts until at $E_\gamma=20$ eV the profile is more heavily weighted towards (π,π). From this they conclude that the true underlying $n(\mathbf{k})$ is symmetric. However, the data in Fig. 9 from 13 different photon energies suggest otherwise. Ten curves have an asymmetry more heavily weighted towards (0,0), three are peaked at $(\pi/2,\pi/2)$, and none are more heavily weighted towards (π,π). Combining Fig. 9(b) with the majority of other single-photon energy studies on SCOC (Refs. 9,19,20,26,27) suggests to us that a true asymmetry does exist in the underlying occupation probability, $n(\mathbf{k})$.

As all of the above studies were only from a single cut through the Brillouin zone we now examine a more global perspective of the intensity profile. Figs. 12(b–f) present relative $n(\mathbf{k})$ patterns of CCOC over a Brillouin-zone quadrant for five different photon energies, while panel (a) is of an optimally doped Bi2212 sample. Spectra are taken at the crosses, values in between were generated from a linear interpolation, and except for panel (c), the data have been symmetrized about $k_x=k_y$ and the geometry of the experimental setup was identical for each data set. The in-plane component of the electric field was polarized along the Cu-O bond direction (This is a 45° rotation relative to the data presented in Figs. 8 and 10). The first two panels reproduce the original comparison of metallic Bi2212 and insulating CCOC from which the initial identification of a ''remnant Fermi surface'' was made.[12] For a state with $d_{x^2-y^2}$ orbital symmetry the suppression of weight as one approaches the line $k_x=0$ is expected. In Bi2212, the only drop in intensity which is not naturally explained by matrix elements is where a Fermi-surface crossing has occurred. As seen in the figure the in-

tensity drop matches the traditional method for determining a Fermi-surface crossing by following the dispersion by eye and is indicated by the dots. This indicates that the surface of steepest descent in the experimentally determined $n(\mathbf{k})$ is a valid method of determining the Fermi surface. The surprise is that a similar drop in intensity is observed in the insulator. Although the feature is less well defined here, the striking resemblance it bears to the metal suggests that the origin is similar, and hence it was qualitatively described as a remnant Fermi surface.[12] (Note that the remnant Fermi surface is still fully gapped by the large Mott gap.)

Here we examine the effect of changing the photon energy to determine if this feature is robust. From panels (b)–(f) one immediately notices that the intensity pattern varies tremendously for the five photon energies: 25.2, 16.5, 29, 32.3, and 41 eV. However, the variations appear predominantly parallel to the $(\pi,0)$ to $(0,\pi)$ direction, while perpendicular to this there exists relatively little variation as we noted above in Fig. 9. The exact shape of the remnant Fermi surface may change, but at all photon energies used there is a loss of spectral weight as one crosses the approximate antiferromagnetic zone boundary from $(0,\pi)$ to $(\pi,0)$. It may appear that the remnant Fermi surface crosses the (0,0) to $(\pi,0)$ cut or the $(\pi,0)$ to (π,π) cut depending on the photon energy chosen, but the broadness and the variability due to matrix elements prevent one from clearly identifying the intensity profile as either case. However, the data clearly suggest that globally there is an asymmetry in intensity stronger towards (0,0) than towards (π,π) as one crosses the region spanned by the black lines in the Brillouin zone, which is coincident with the antiferromagnetic zone boundary.

Although the $n(\mathbf{k})$ image plots can provide a wealth of information and are extremely good for summarizing the data, it is to also important look at the raw data to fully appreciate the information being given by the image plots. This is done in Fig. 13. Panels (a) and (b) plot, respectively, the EDC's from (0,0) to (π,π) and $(\pi/2,\pi/2)$ to $(\pi,0)$, from the data sets used to create the intensity maps in Figs. 12(b–f). We find that the spectra are qualitatively similar. This is true even at 41 eV, where the peak is poorly defined throughout the zone. To examine them more closely, Fig. 14 plots both the dispersion of the peak position and $n(\mathbf{k})$ together for all the cuts along the antiferromagnetic zone boundary. Similar to the nodal direction shown in Fig. 9(a), only slight differences exist in dispersion, $E(\mathbf{k})$, among the five different photon energies. However, the spectral intensity, $n(\mathbf{k})$, varies seemingly randomly with photon energy. In the extreme case between 25.2 eV and 29 eV the intensity is increasing as one approaches $(\pi/2,\pi/2)$ for the former, and decreasing for the latter. One might expect such behavior when the underlying spectral function does not possess an asymmetry. Meanwhile, the asymmetry in spectral weight perpendicular to the antiferromagnetic zone boundary [see Fig. 9(b)] appears robust to the strong variations in the matrix element.

In general, the outgoing photoelectrons resulting from photons with different wavelengths will necessarily have a different overlap with the initial wave functions of the system, and hence different cross sections. This is impossible to
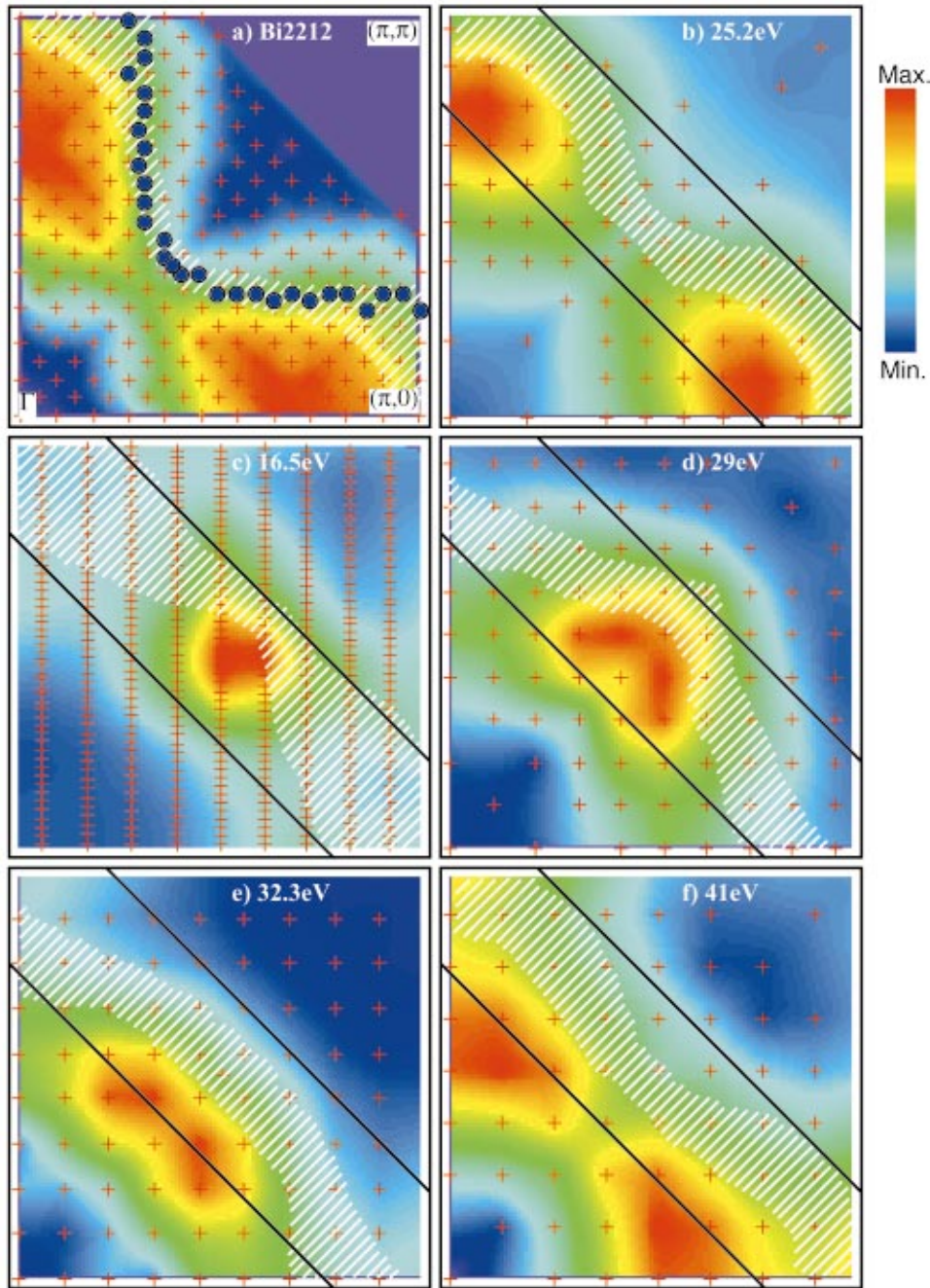
FIG. 12. (Color) Integrated spectral weight. The crosses indicate where spectra were taken. Except for (c) the data are symmetrized about the $k_x = k_y$ line. Red is maximum. (a) Optimally doped Bi2212 at $E_\gamma = 22.4$ eV. The white hashed region indicates the approximate location of the Fermi surface determined from $n(\mathbf{k})$. The dots illustrate the position of the Fermi surface as determined by the traditional method for analyzing ARPES data. (b) CCOC shows a striking similarity to the metal allowing the identification of the white hashed region as a remnant Fermi surface. Comparison of (b)–(f) shows CCOC taken at photon energies of 25.2, 16.5, 29, 32.3, and 41 eV. The intensity maxima vary between different panels, but the loss of intensity as one approximately crosses the antiferromagnetic zone boundary is a consistent feature. The cumulative boundary of the remnant Fermi surface is drawn with black lines on panels (b)–(f). Resolution $\Delta E \leq 70$ meV.

avoid. Ideally, to eliminate such matrix element effects one would average over all possible photon energies, and experimental geometries. Here we have observed large variations along the antiferromagnetic zone boundary, which are clear manifestations of the matrix element, while the asymmetric shift of weight towards (0,0) with respect to the $(\pi,0)$ to $(0,\pi)$ line suggests that this is a property of the underlying spectral function. Our initial report implied that the underlying $n(\mathbf{k})$ structure matched that of the local-density approximation (LDA) Fermi surface at half filling without correlations.[12] It is now clear that the matrix elements are strong enough to make such a precise identification very difficult. However, we verify that an underlying asymmetry exists in the spectral function about the antiferromagnetic zone

boundary, which is robust despite variations with photon energy. Whether it truly lies along the LDA Fermi surface, the antiferromagnetic zone boundary, or some other contour is a more difficult question to answer.

VIII. ROUNDED NODAL DISPERSION

The greatest utility of the remnant Fermi-surface concept as it pertains to the high-temperature superconductors is that a d-wave-like dispersion was identified in the insulator, which could thus provide a natural connection to the d-wave-like high-energy pseudogap.[12] In ARPES the pseudogap about $(\pi,0)$ is characterized in two ways. The first is by the use of the leading edge midpoint, which has the same energy
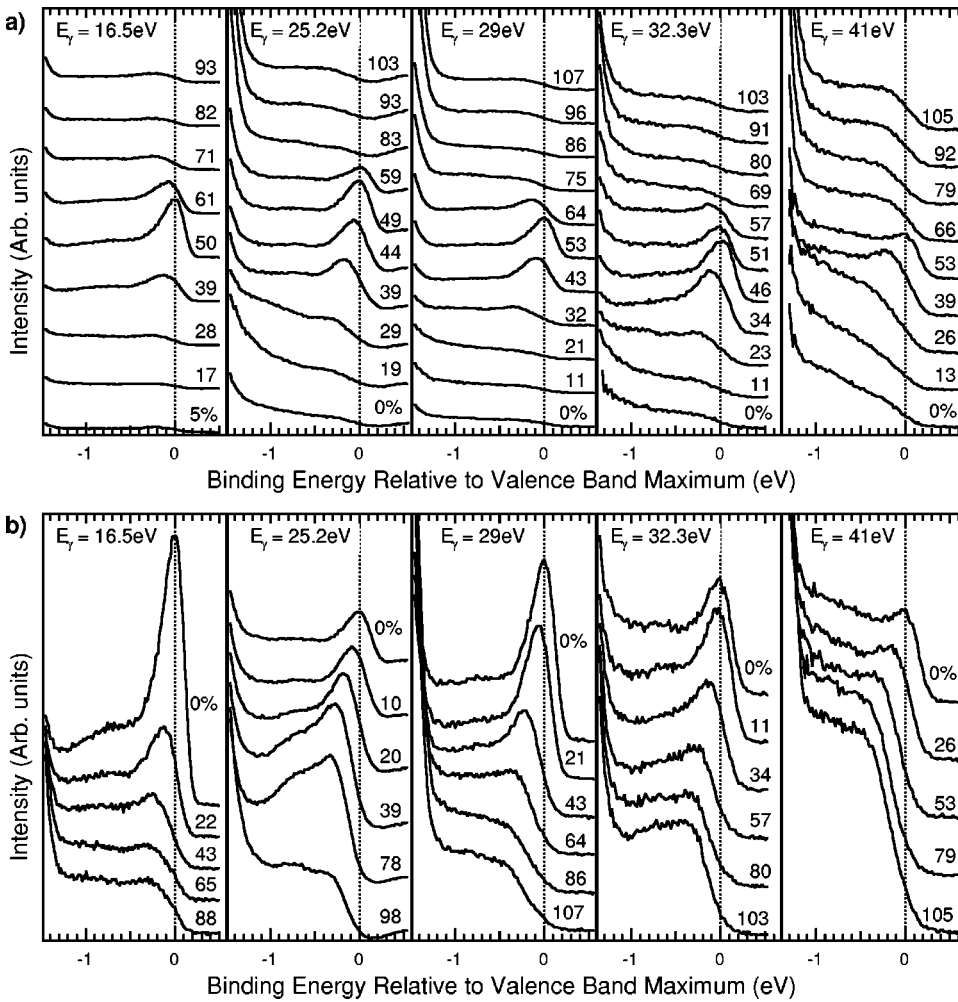
FIG. 13. ARPES spectra along two cuts, (a) (0,0)(bottom) to (π,π) (top) and (b) ($\pi/2,\pi/2$) (top) to (π,0) (bottom), with five different photon energies (16.5, 25.2, 29, 32.3, and 41 eV). The numbers refer to the percentage distance along each cut. The intensities of the features vary, but the dispersion remains the same.

scale as the superconducting gap, and is typically defined in the same way, only above T_c. However, another energy scale exists in the spectra which is an order of magnitude larger, and is sometimes refered to as a hump or a high-energy pseudogap. This is the feature which provides a direct connection with the dispersion observed in the insulator.[32] The remnant Fermi surface identifies a topological contour in the Brillouin zone of the insulator, which in this case is the antiferromagnetic zone boundary. By examining the dispersion along this contour one can identify a "gap" in this system, the dispersion of which along the remnant Fermi surface fits the d-wave functional form remarkably well. We now extend our earlier study on CCOC to examine the precise nature of the dispersion near the nodal line $k_x=k_y$.[12] A simple d-wave dispersion proportional to $|\cos k_x a - \cos k_y a|$ would produce a linear dispersion with a discontinuous derivative perpendicular to the nodal direction at $k_x=k_y$. This is most easily seen along the antiferromagnetic zone boundary where the above
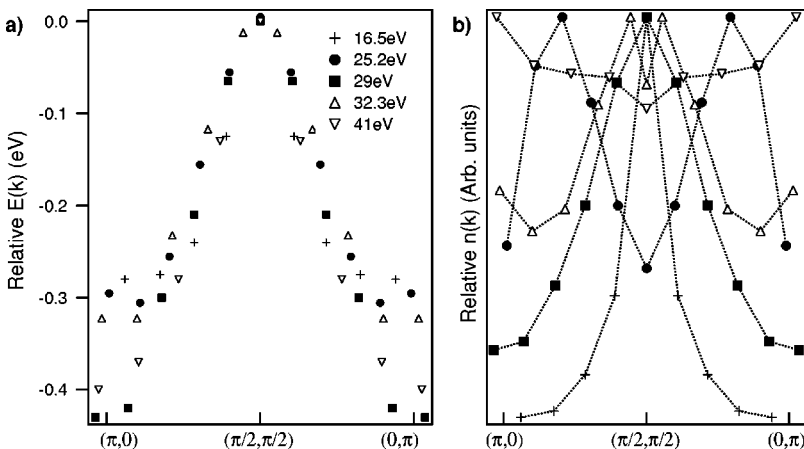

FIG. 14. (a) Peak position and (b) $n(\mathbf{k})$ from the spectra in Fig. 13 along the antiferromagnetic zone boundary. The data along (π,0) to (0,π) have been symmetrized. Again the dispersion is independent of photon energy, while the intensity varies randomly indicating that this modulation in intensity is solely due to matrix elements.
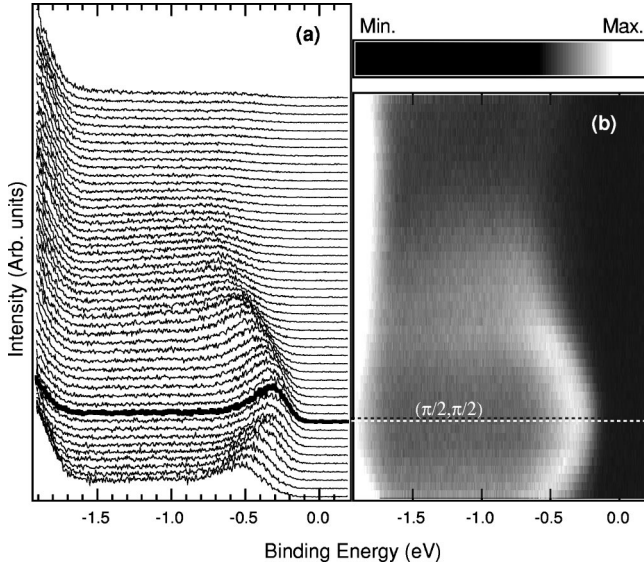
FIG. 15. (a) EDC's and (b) corresponding image plot of $Ca_2CuO_2Cl_2$ data taken along the antiferromagnetic zone boundary at 0.6° intervals. ($\pi/2, \pi/2$) is indicated by the bold EDC and the dotted line in the image plot. Data collected at $T = 200$ K, 25.5 eV photons, resolution $\Delta E = 15$ meV, and 0.8° angular resolution.
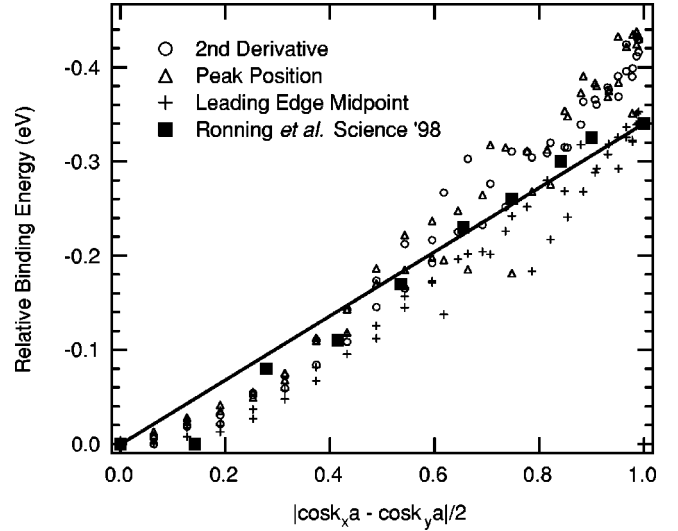

FIG. 16. Examining the curvature about the nodal line using three methods for characterizing the dispersion of the data in Fig. 15 plotted with the original data from Ref. 12. A straight line corresponds to a simple d-wave dispersion. Each curve was set to zero relative binding energy at the node. Note that the d-wave-like gap is in addition to the Mott gap which is not shown. The increased scatter as one approaches ($\pi, 0$) is indicative of the increased difficulty in tracing the dispersion away from ($\pi/2, \pi/2$).

function reduces to $|\sin(k_x a - \pi/2)|$. Such a nonanalytic dispersion is nontrivial, and hence the presence or absence of such a dispersion is of great significance to theories that attempt to unify the antiferromagnetic insulator with the d-wave superconductor.

In Fig. 15 we present EDC's taken at 0.6° intervals along the antiferromagnetic zone boundary and through ($\pi/2, \pi/2$). One observes a smooth round dispersion through ($\pi/2, \pi/2$). This is even more evident in the image plot of the same data. To compare with the d-wave functional form we must quantify the dispersion seen in the raw spectra. The low-energy features seen in the insulator are inherently very broad with a full width at half maximum at ($\pi/2, \pi/2$) of 300 meV, which is roughly the total dispersion seen in this material. Due to this, and the fact that the higher-energy spectral weight is also dispersive and of unknown origin, the significance of any particular fit to the data is questionable. For this reason we have chosen to quantify the dispersion using three methods: the peak maximum, the location of maximum curvature, and the leading edge midpoint. We compare these quantities against $|\cos k_x a - \cos k_y a|$ in Fig. 16. The straight line represents the simple d-wave scenario. Near the node it is clear that the dispersion is rounded in each case.

One plausible explanation for the flatness of the dispersion near ($\pi/2, \pi/2$) could be the dirty d-wave scenario. Previous ARPES work on underdoped Bi2212 samples also found a flattened dispersion near the node of the superconducting and normal-state low-energy pseudogaps.[33–35] Earlier works suggested that this was consistent with a dirty d-wave scenario, since a finite density of states with zero excitation energy would result in a flattening of the node region. However, Mesot *et al.* argued that flattening due to impurities can be ruled out since pair breaking due to impurities should cause the overall magnitude of the gap to de-

crease, while they observed the opposite.[35] Furthermore, we note that ACOC is very stable and most likely very chemically pure as evidenced by many unsuccessful attempts by many groups to dope the oxychlorides under atmospheric conditions.[36] The broadness of the peaks cannot be used as an evidence for impurities since the same feature is almost equally broad in Bi2212 samples, which contain nearly resolution limited quasiparticle peaks in their spectra in the superconducting state.[37] Although one cannot rule out the possibility that the observed dispersion is due to impurities we will, for the remainder of this paper, assume that the observed rounding is intrinsic to the undoped insulator, and discuss the consequences. We defer a full discussion on the line shape of the insulator to another paper.[38]

In an attempt to quantify the deviation from a simple d-wave picture we fit the data to $\Delta |B\cos(2\phi) + (1 - B)\cos(6\phi)|$ in Fig. 17, where ϕ is defined in the figure, $\cos(2\phi)$ is approximately $|\cos k_x a - \cos k_y a|$, and $\cos(6\phi)$ is the next allowable harmonic for d-wave symmetry. An increase in the $\cos(6\phi)$ weight (smaller B) corresponds to a flatter nodal region. Experimentally, we find $B = 0.81 \pm 0.01$. This is smaller than any underdoped sample measured by Mesot *et al.*, and thus is consistent with their interpretation that the rounding is a result of increasing antiferromagnetic correlations.[35]

Finally, we note that the above data were taken at $E_\gamma = 25.5$ eV. Identical results were obtained at $E_\gamma = 29$ eV, on a second cleave of CCOC at $E_\gamma = 25.5$ eV, and on SCOC using 22.4 eV photons. Improving the angular resolution by a factor of 4 by narrowing the slits of our analyzer produced the same results.
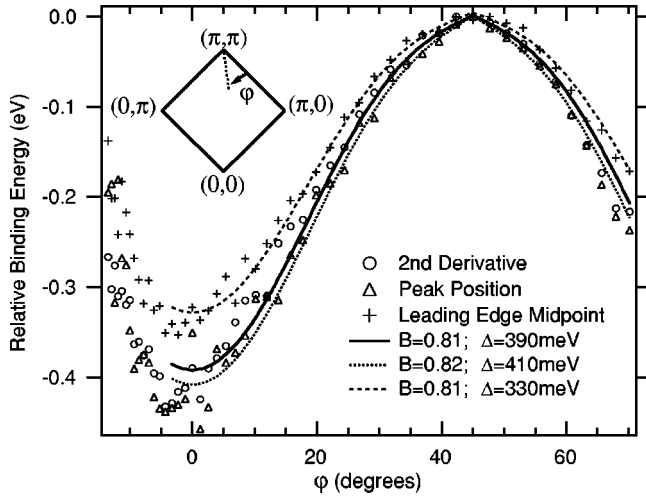
FIG. 17. Fits of the data presented in Fig. 16 to $\Delta|B\cos(2\phi)+(1-B)\cos(6\phi)|$, where ϕ is indicated in the figure. B characterizes the deviation from a simple d-wave.

IX. DISCUSSION

A. System independence

By examining $A_2CuO_2X_2$, ($A=$Sr, Ca; $X=$Cl, Br) and $Bi_2Sr_2MCu_2O_8$ ($M=$Er, Dy) we found that the dispersion of the lowest-lying excitations in parent cuprates are independent of the particular system studied. Even the results of the Cu_3O_4 system, $Sr_2Cu_3O_4Cl_2$, were similar to the half-filled CuO_2 systems. We further note that, $Nd_{2-x}Ce_xCuO_4$ and $La_{2-x}Sr_xCuO_4$ near half filling have been studied as well.[2,3,39] For Nd_2CuO_4 a shoulder on the edge of the valence band exists and exhibits a minimum binding energy at $(\pi/2,\pi/2)$.[3] Perhaps this is the strongest evidence supporting the independence of the low-energy electronic structure of half-filled cuprates on the apical site, as it is completely unoccupied in Nd_2CuO_4. In La_2CuO_4, a broad shoulder exists at $(\pi/2,\pi/2)$ at 0.5 eV which disperses by roughly 200 meV to higher binding energy as it approaches $(\pi,0)$.[2,39] It is also interesting to note that the exchange coupling J, which enters into the parametrization of the low-energy electronic structure, is nearly equivalent in La_2CuO_4 (135 meV) and $Sr_2CuO_2Cl_2$ (125 meV) as determined from inelastic neutron and two-magnon Raman scattering.[40] All of these observations further support the universality to all cuprates of the dispersion of the lowest-energy feature seen in $Sr_2CuO_2Cl_2$ and $Ca_2CuO_2Cl_2$.

The role of crystallographic structure on the low-energy electronic structure and superconductivity is still not well established. It was believed that the apical oxygen or structural distortion of the CuO_2 planes was necessary for superconductivity, but the observation of superconductivity in Na-doped $Ca_2CuO_2Cl_2$ and $Sr_2CuO_2F_{2+\delta}$ has since rejected these beliefs.[41,42] In Na-doped $Ca_2CuO_2Cl_2$ no structural distortion was found down to 10 K, while superconductivity was observed as high as 26 K. Perhaps the apical Cl stabilizes a structure with an increased Cu-O-Cu distance relative to systems with an apical oxygen. Clearly this is not significant enough to eliminate superconductivity in CCOC with an

a-axis lattice constant of 3.87 Å, but may be responsible for the fact that SCOC, with $a=3.97$ Å has not yet been successfully doped into a superconductor.[6] Although band structure claims that the apical halide ion does not appreciably enter the low-energy density of states of superconducting oxyhalides,[43] one should note that hole-doped superconductivity is observed in compounds containing an apical anion, while electron-doped superconductivity is found in systems missing an apical atom. This suggests that the role of the apical atom is not completely understood.

B. E_γ dependence

Returning to the photon energy dependence of the cuprates, let us first consider the independence of the observed dispersion $E(\mathbf{k})$ on the choice of photon energy. In principle, there are several reasons which could cause $E(\mathbf{k})$ to depend on photon energy, which we list below. We know that the cuprates are generally believed to be two-dimensional electronic systems. In reality the wave functions have some finite $\mathbf{z}$ extent, and even if they are highly localized they will have some finite overlap with neighboring planes. In fact, such a coupling must be present to create the observed three-dimensional long-range magnetic order seen at half filling. Certainly, if the wave-function overlap were large enough to create a small dispersion as a function of k_z, a change in dispersion would be observed with changing photon energy as this varies k_z. Alternatively, if the matrix element had a significant dependence in the binding energy of the feature which varied with photon energy, a photon energy dependent dispersion would also result. Along similar reasoning, if there are multiple excitation branches then there is no reason to expect that the matrix element dependence on photon energy would be the same for each branch. Most likely an observed variation with photon energy would be caused by a combination of several of these factors. However, in Figs. 9 and 14 we have shown that the dispersion of the insulator is independent of photon energy within our experimental uncertainty. Three dimensionality may still play a role in causing a small shift in dispersion with photon energy, but not surprisingly, it is a safe assumption to treat the electronic structure of this half-filled insulator as essentially two dimensional.

What then is the significance of the observed underlying intensity modulation along the nodal direction, which appears robust to variations in photon energy? In the context of specific many-body models such as the Hubbard model, there is numerical evidence that a structure in $n(\mathbf{k})$ survives even when the on site Coulomb U drives the system insulating, even though the discontinuity in $n(\mathbf{k})$ which existed in the metal has been washed out.[28,30,44] This effect is linked to the fact that $n(\mathbf{k})$ reflects the underlying Fermi statistics of the electronic system, where for the specific case of a two-dimensional square lattice that resembles the CuO_2 planes of the cuprates, there is a drop in $n(\mathbf{k})$ across a line that is close to the antiferromagnetic zone boundary.[28,30] This differs in the generalized t-J models where the structure in $n(\mathbf{k})$ is washed out.[30,45]

In the metallic state of optimally doped Bi2212 the steepest descent of $n(\mathbf{k})$ gives a Fermi surface consistent with

traditional ARPES analysis methods despite the complication of matrix element effects as shown in Fig. 12. In our earlier paper,[12] the $n(\mathbf{k})$ pattern of the insulator CCOC was found to be strikingly similar to the $n(\mathbf{k})$ pattern seen in Bi2212. This realization, coupled with many-body theoretical calculations on various forms of the Hubbard model,[28,30] suggests that the insulator pattern contains information that is related to a Fermi surface which has been destroyed by strong electron-electron interactions thus giving a qualitative concept of a remnant Fermi surface as the surface of steepest descent in $n(\mathbf{k})$. In this paper, we have found that the remnant Fermi surface acts to emphasize a robust feature which we observe in the insulator, although its precise shape is uncertain due to the effects of the matrix elements. While this may not be a rigorous definition, as the Fermi surface is only defined for a metal, this useful concept allows a practical connection from the pseudogap seen in underdoped cuprates to the properties of the insulator.[13]

Unfortunately, the fact that the antiferromagnetic Brillouin-zone boundary is quite similar to the underlying Fermi surface means that the roles of magnetism and that of the Fermi statistics of the underlying band structure in this spectral weight pattern will be uncertain. Therefore, we suggest here a few ideal tests on the origin of the $n(\mathbf{k})$ pattern. One idea is to study a system whose noninteracting Fermi surface is radically different from the magnetic Brillouin-zone boundary. Since such a system compatible with ARPES may be difficult to find, perhaps a more realistic approach will be to study a system similar to the cuprates, but where the magnetic correlations are much smaller, such that at the measured temperature, effects due to magnetic correlations could be ruled out.

We have shown that the loss in intensity as one crosses the antiferromagnetic zone boundary is a robust feature of the insulator $Ca_2CuO_2Cl_2$, which cannot be explained solely by matrix element effects. However, the photon energy dependence underscores the qualitative rather than quantitative nature of the remnant Fermi-surface concept. We argue that much physics can be learned in spite of the adverse effects which matrix elements can have in ARPES, as long as care is taken to properly sort out the intrinsic versus the extrinsic physics. In particular, the resulting connection between the d-wave-like dispersion and the pseudogap in the underdoped regime is robust.

C. *d*-wave-like dispersion

Let us now address the significance of the rounded dispersion at $(\pi/2,\pi/2)$. Numerical calculations show that the t-J model describes the dispersion from $(0,0)$ to (π,π) well, but incorrectly predicts the energy at $(\pi/2,\pi/2)$ and $(\pi,0)$ to be equal.[28] The addition of t' and t'' corrects this problem[46] and for realistic values of these parameters, also gives an isotropic dispersion which is scaled by a single parameter J.[47] The effect of adding t' and t'' to calculations is to destabilize the single-hole Néel state about $(\pi,0)$. The resulting state appears to be a spin liquid which may display spin charge separation, but this only occurs about $(\pi,0)$.[47,48] Perhaps this explains why resonating valence bond theories,
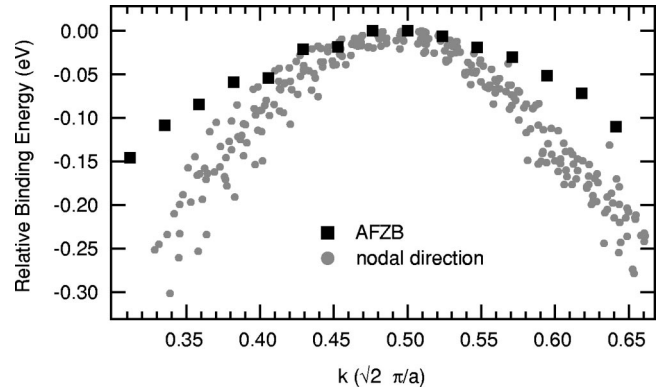

FIG. 18. Anisotropy of the dispersion about $(\pi/2,\pi/2)$. The nodal direction data are reproduced from Fig. 9, including all 13 photon energies at once, while the data along the antiferromagnetic zone boundary (AFZB) are reproduced from Fig. 17. The dispersion in each case is found by taking the minimum of the second derivative of the respective EDC's.

which assume spin charge separation throughout the entire zone, incorrectly predict a cusp at $(\pi/2,\pi/2)$ in the spinon dispersion while still correctly describing the overall dispersion on a qualitative level.[13,15]

The mean-field treatment in a simple spin density wave picture applied to the Hubbard model with up to third nearest-neighbor hopping fails to describe the data.[47] The dispersion along $(\pi,0)$ to $(0,\pi)$ is much too great for realistic parameters. However, the dispersion does contain a rounded nodal region. If one can argue that one should renormalize these parameters then it is possible to obtain a very good fit to the experimental data as done by Nuñez-Regueiro[49] where they also show that the magnitude of the overall dispersion decreases with doping as has been seen in the high-energy pseudogap. Alternatively, a diagrammatic expansion of the Hubbard model containing t' and t'' as well as the QED_3 theory also reproduce the observed dispersion.[50,51] Finally, the SO(5) theory predicts a $|\cos k_x a - \cos k_y a|$ dispersion for the insulator when the superconductor has simple d-wave pairing.[16] However, in the projected SO(5), the observed flattening of the node in the insulator is consistent with a flattened dispersion observed near the node of the superconducting gap.[52]

D. E_k isotropy of $(\pi/2,\pi/2)$

By combining our investigation of the nodal direction with that of the rounding along the antiferromagnetic zone boundary we can get a measure of the isotropy of the dispersion at $(\pi/2,\pi/2)$ shown in Fig. 18. The data demonstrate a clear anisotropy in the two directions. However, it should be noted that in tracking the dispersion from the EDC's the total dispersion in both directions does not exceed 350 meV. It is only due to the improved momentum resolution that we get a clear indication of the existence of some anisotropy in the dispersion about $(\pi/2,\pi/2)$. It should be noted that the full dispersion in the nodal direction is difficult to extract due to a loss of spectral weight at $(0,0)$, which has historically been attributed to matrix elements. A similar lack of spectral

weight near $(\pi,0)$ exists in SCOC, but for CCOC the total dispersion along the antiferromagnetic zone boundary is easily extracted (see Fig. 1). The resulting 350-meV dispersion agrees with the estimates determined from SCOC. We note that most models can easily account for a small degree of anisotropy by introducing additional terms such as next nearest-neighbor hopping.

X. CONCLUSIONS

To summarize, we have studied the Mott-insulating cuprates: $Sr_2CuO_2Cl_2$, $Ca_2CuO_2Cl_2$, $Ca_2CuO_2Br_2$, $Sr_2Cu_3O_4Cl_2$, $Bi_2Sr_2ErCu_2O_8$, and $Bi_2Sr_2DyCu_2O_8$. The lowest-energy excitations measured by ARPES are the same in these compounds as for the prototypical insulators: $Sr_2CuO_2Cl_2$ and $Ca_2CuO_2Cl_2$. Other studies on $La_{2-x}Sr_xCuO_4$ and Nd_2CuO_4 have similar results.[2,3,39] This shows that the low-energy excitations are indeed independent of the apical atom, and that the results from $Sr_2CuO_2Cl_2$ and $Ca_2CuO_2Cl_2$ are truly representative of a half-filled CuO_2 plane. This justifies the connection between the high-energy pseudogap observed in underdoped Bi2212 and the d-wave-like modulation seen in ACOC.[12,13] Our photon energy dependent study enables us to extract the intrinsic spectral function, which shows that the dispersion is indeed independent of photon energy, and that despite strong variations due to the matrix elements an asymmetry exists in the $n(\mathbf{k})$ about the line from $(\pi,0)$ to $(0,\pi)$. We find that the dispersion along this contour does not fit a simple d-wave dispersion, but is flattened near $(\pi/2,\pi/2)$ consistent with a similar rounding observed in underdoped Bi2212 samples.[33–35] Numerical calculations on the t-t'-t''-J model, which match all aspects of the insulator dispersion including the rounded nodal region, show that the antiferromagnetic correlations are destroyed near $(\pi,0)$, indicating that a spin liquid picture may be more appropriate for interpreting the ARPES data.[47,48] However, generalized t-J models fail to reproduce the observed asymmetric intensity profile which is reproduced in the Hubbard model.[28,30] Possibly the Hubbard model including the next nearest-neighbor hopping terms[50] is necessary to capture all the physics of a single hole in the half-filled CuO_2 plane.

*Present address: Dept. of Physics, University of Toronto, 60 St. George St, Toronto, ON, Canada M5S 1A7.

†Present Address: Dept. of Physics, Yonsei University, Seoul, Korea.

§Present Address: Dept. of Physics and Astronomy, UCLA, Los Angeles, CA.

‡Present Address: Dept. of Physics and Astronomy, University of British Columbia, Vancouver, Canada

[1] N.F. Mott, Proc. Phys. Soc., London, Sect. A **62**, 416 (1949).

[2] A. Ino *et al.*, Phys. Rev. B **62**, 4137 (2000).

[3] N.P. Armitage *et al.*, Phys. Rev. Lett. **88**, 257001 (2002).

[4] N. Harima *et al.*, Phys. Rev. B **64**, 220507 (2001).

[5] M.C. Schabel *et al.*, Phys. Rev. B **57**, 6090 (1998).

[6] B. Grande and H. Müller-Buschbaum, Z. Anorg. Allg. Chem. **417**, 68 (1975).

[7] D.W. Lynch and C.G. Olson, *Photoemission Studies of High-Temperature Superconductors* (Cambridge University Press, Cambridge, London, 1999).

[8] F.C. Zhang and T.M. Rice, Phys. Rev. B **37**, 3759 (1988).

[9] S. Haffner *et al.*, Phys. Rev. B **61**, 14 378 (2000).

[10] C. Dürr *et al.*, Phys. Rev. B **63**, 014505 (2000).

[11] S. Haffner *et al.*, Phys. Rev. B **63**, 212501 (2001).

[12] F. Ronning *et al.*, Science **282**, 2067 (1998).

[13] R.B. Laughlin, Phys. Rev. Lett. **79**, 1726 (1997).

[14] P.J. White *et al.*, Phys. Rev. B **54**, R15 669 (1996).

[15] Z.Y. Weng *et al.*, Phys. Rev. B **63**, 075102 (2001).

[16] S. Rabello *et al.*, Phys. Rev. Lett. **80**, 3586 (1998).

[17] L.L. Miller *et al.*, Phys. Rev. B **41**, 1921 (1990).

[18] T. Kitajima *et al.*, J. Phys.: Condens. Matter **11**, 3169 (1999).

[19] B.O. Wells *et al.*, Phys. Rev. Lett. **74**, 964 (1995).

[20] C. Kim *et al.*, Phys. Rev. Lett. **80**, 4245 (1998).

[21] L.F. Mattheiss, Phys. Rev. B **42**, 354 (1990).

[22] D.S. Marshall *et al.*, Phys. Rev. Lett. **76**, 4841 (1996).

[23] Z.-X. Shen and D.S. Dessau, Phys. Rep. **253**, 1 (1995).

[24] M.S. Golden *et al.*, Phys. Rev. Lett. **78**, 4107 (1997).

[25] H.C. Schmelz *et al.*, Phys. Rev. B **57**, 10 936 (1998).

[26] J.J.M. Pothuizen *et al.*, Phys. Rev. Lett. **78**, 717 (1997).

[27] S. LaRosa *et al.*, Phys. Rev. B **56**, R525 (1997).

[28] E. Dagotto, Rev. Mod. Phys. **66**, 763 (1994).

[29] E. Dagotto *et al.*, Phys. Rev. B **41**, 9049 (1990); Z. Liu and E. Manousakis, *ibid.* **45**, 2425 (1992).

[30] H. Eskes and R. Eder, Phys. Rev. B **54**, 14 226 (1996).

[31] M. Randeria *et al.*, Phys. Rev. Lett. **74**, 4951 (1995).

[32] For a review on ARPES of cuprates including a discussion of the pseudogaps see: A. Damascelli, Z.-X. Shen, and Z. Hussain, Rev. Mod. Phys. (to be published); http: //xxx.lanl.gov/cond-mat/0208504.

[33] A.G. Loeser *et al.*, Science **273**, 325 (1996).

[34] J.M. Harris *et al.*, Phys. Rev. B **54**, R15 665 (1996).

[35] J. Mesot *et al.*, Phys. Rev. Lett. **83**, 840 (1999).

[36] Y. Kohsaka, Masters thesis, University of Tokyo, 2001.

[37] A. Kaminski *et al.*, Phys. Rev. Lett. **84**, 1788 (2000).

[38] C. Kim *et al.*, Phys. Rev. B **65**, 174516 (2002).

[39] T. Yoshida *et al.*, http//xxx.lanl.gov/cond-mat/0206469 (unpublished).

[40] M.A. Kastner *et al.*, Rev. Mod. Phys. **70**, 897 (1998).

[41] Z. Hiroi, N. Kobayashi, and M. Takano, Nature (London) **371**, 139 (1994); Z. Hiroi, N. Kobayashi, and M. Takano, Physica C **266**, 191 (1996).

[42] M. Al-Mamouri *et al.*, Nature (London) **369**, 382 (1994).

[43] D.L. Novikov, A.J. Freeman, and J.D. Jorgensen, Phys. Rev. B **51**, 6675 (1995).

[44] N. Bulut, D.J. Scalapino, and S.R. White, Phys. Rev. Lett. **73**, 748 (1994).

[45] F. Lema and A.A. Aligia, Phys. Rev. B **55**, 14 092 (1997).

[46] T. Tohyama and S. Maekawa, Supercond. Sci. Technol. **13**, R17 (2000), and references therein.

[47] T. Tohyama *et al.*, J. Phys. Soc. Jpn. **69**, 9 (2000).

[48] G.B. Martins, R. Eder, and E. Dagotto, Phys. Rev. B **60**, R3716 (1999).

[49] M. D Nuñez-Regueiro, Eur. Phys. J. B **10**, 197 (1999).

[50] P. Brune and A.P. Kampf, Eur. Phys. J. B **18**, 241 (2000).

[51] I.F. Herbut, Phys. Rev. B **66**, 094504 (2002).

[52] M.G. Zacher *et al.*, Phys. Rev. Lett. **85**, 824 (2000).